Proton NMR Investigation of the Oxidized Three-Iron Clusters in the Ferredoxins from the Hyperthermophilic Archae *Pyrococcus furiosus* and *Thermococcus litoralis*†

Scott C. Busse,‡ Gerd N. La Mar,*,‡ Liping P. Yu,‡ James B. Howard,§ Eugene T. Smith,∥ Zhi Hai Zhou,∥ and Michael W. W. Adams∥

Department of Chemistry, University of California, Davis, California 95616, Department of Biochemistry, University of Minnesota, Minneapolis, Minnesota 55455, and Department of Biochemistry and Center for Metalloenzyme Studies, University of Georgia, Athens, Georgia 30602

Received July 14, 1992; Revised Manuscript Received September 24, 1992

ABSTRACT: The 3Fe forms of ferredoxins (Fd) from the hyperthermophilic archaebacteria *Pyrococcus furiosus* (*Pf*) and *Thermococcus litoralis* (*Tl*) have been investigated by ^{1}H NMR. A combination of one-dimensional nuclear Overhauser and two-dimensional NOESY and bond correlation spectroscopy provides the assignment of the aromatic residues, one conserved valine, and the location of the signals for each of the three cysteines coordinated to the clusters. Dipolar contacts between the Trp 2 and Tyr 46 in *Pf* Fd and from an invariant phenylalanine to an invariant valine and a cluster cysteine in both Fd confirm a folding pattern for these proteins that is very similar to that of the crystallographically characterized ferredoxin from the mesophile *Desulfovibro gigas*. The sequence-specific assignment of the buried cysteine near the invariant phenylalanine has been made. The temperature dependence of the contact-shifted cysteinyl residues reveals a distinct 2:1 asymmetry in the magnetic coupling among the three high-spin ferric ions, in that one cysteine exhibits Curie behavior, while the other two cysteines display anti-Curie behavior. These magnetic properties are rationalized qualitatively on the basis of a magnetic coupling scheme where two iron couple to yield an intermediate spin of 2 which couples to the remaining $S = 5/2$ iron to yield the total cluster spin 1/2. This magnetic asymmetry appears to be a characteristic feature of oxidized 3Fe clusters. *Pf* Fd also undergoes a dynamic equilibrium between two alternate forms that differ slightly in the environment of two of the coordinated cysteines. Analysis of the pattern of the contact shifts for the three cysteines in the two ferredoxins suggests that the cysteine coordinated to the unique iron does not have the same sequence origin.

Iron–sulfur clusters in proteins fulfill diverse chemical functions yet utilize a relatively limited number of fundamental structures, namely, $[Fe_2S_2]^{1+,2+}$, $[Fe_3S_4]^{0,1+}$, $[Fe_4S_4]^{1+,2+,3+}$ clusters [for reviews, see Lovenberg (1973), Spiro (1982), Thompson (1985), Beinert, (1990), and Howard and Rees (1991)]. All iron atoms are tetrahedrally coordinated to bridging sulfur atoms and terminal cysteinyl ligands and are high-spin but magnetically coupled in all known cluster oxidation states. In the 2Fe clusters, the iron retain formal valence states (i.e., Fe^{3+}-Fe^{3+} for oxidized and Fe^{3+}-Fe^{2+} for reduced yielding total $S = 0$ and $S = 1/2$ ground states, respectively) (Gibson et al., 1966; Fee et al., 1984; Johnson, 1986), whereas the 4Fe systems have some pairs of iron atoms exhibiting "delocalized" or averaged valence states of $Fe^{2.5+}$ (i.e., $2Fe^{2.5+}$-$2Fe^{2.0+}$, $2Fe^{2.5+}$-$2Fe^{2.5+}$, and $2Fe^{2.5+}$-$2Fe^{3.0+}$, for the three known oxidation states with spin ground states $S_T = 1/2$, 0, and 1/2, respectively) (Moss et al., 1968; Dickson et al., 1974; Cammack et al., 1977; Middleton et al., 1978, 1980). For 3Fe clusters in the oxidized (+1) form, three high-spin ferric ions couple to yield a total spin ground state of 1/2. Hence, Mössbauer and magnetic susceptibility studies indicate idential iron environments (Huynh et al., 1980; Emptage et al., 1980; Moura et al., 1982; Day et al., 1988) although low-temperature ESR data have been interpreted as reflecting a 2:1 asymmetry in the coupling scheme (Kent et al., 1980). When the cluster is reduced, the added electron is delocalized over a specific or "special" pair of Fe which in turn couple to the remaining Fe^{3+} for a cluster spin of $S = 2$ (Thompson et al., 1981; Papaefthymiou et al., 1987; Münck et al., 1988).

Delocalized valence states are therefore characteristic of both 3Fe and 4Fe clusters, but little is known about how the protein structure controls the differentiation between the iron pairs. ^{1}H NMR is uniquely suited for studying both the electronic/magnetic properties of the individual iron atoms of a cluster and the overall protein structure. The observed contact shifts for the β-methylene protons of the coordinated cysteine reflect both the spin magnetization, $\langle S_z \rangle_i$, for the individual iron atom, i, as well as the orientation of the methylene protons relative to the iron atom, i.e.

$$\delta_{con}{}^{i} = (b_o + b_2 \cos^2 \varphi) D \langle S_z \rangle_i \qquad (1)$$

where b_o, b_2, and D are constants and φ is the angle between the Fe–S–C_β plane and the p orbital with the unpaired spin (Poe et al., 1970; Busse et al., 1991). A spin Hamiltonian formulation of the exchange coupling in 2Fe and 4Fe clusters has been fruitfully applied to identify the characteristic temperature dependence for the ferric and ferrous ions in 2Fe clusters (Dunham et al., 1991; Banci et al., 1990), as well as the valence delocalized pair in both the $[Fe_4S_4]^{1+,3+}$ states of 4Fe clusters (Bertini et al., 1991b, 1992). One- and two-

† This research was supported by grants from the National Science Foundation, DMB-91-04018 (G.N.L.), DMB-91-20515 (J.B.H.), and DMB-91-05150 (M.W.W.A.). The NMR instrumentation was purchased in part, with funds provided by the National Institutes of Health, RR-04795, and National Science Foundation, BBS-88-04739.

‡ University of California.
§ University of Minnesota.
∥ University of Georgia.

0006-2960/92/0431-11952$03.00/0

```
      1                  10                  20                  30
                           I    II    III      V
Pf    A-W-K-V-S-V-D-Q-D-T-C-I-G-D-A-I-C-A-S-L-C-P-D-V-F-E-M-N-D-E-
Tl      M-K-V-S-V-D-K-D-A-C-I-G-C-G-V-C-A-S-I-C-P-D-V-F-E-M-D-D-D-
Dg        P-I-E-V-N-D-D-  C-M-A-C-E-A-C-V-E-I-C-P-D-V-F-E-M-N-E-E-

                         40                  50                  60
                                            VI                IV
Pf    G-K-A-Q-P-K-V-E-V-I-E-D-E-E-L-Y-N-C-A-K-E-A-M-E-A-C-P-V-S-A-
Tl    G-K-A-    K-A-  L-V-A-E-T-D-L-  E-C-A-K-E-A-A-E-S-C-P-T-G-A-
Dg    G K-A-      V-  V-I-N D-S-D-L-  D-C-V-E-E-A-I-D-S-C-P-A-E-A-
       D                   P

Pf    I-T-I-E-E-A
Tl    I-T-V-E
Dg    I-V-R-S
```

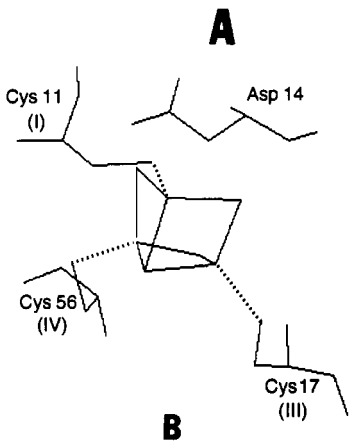

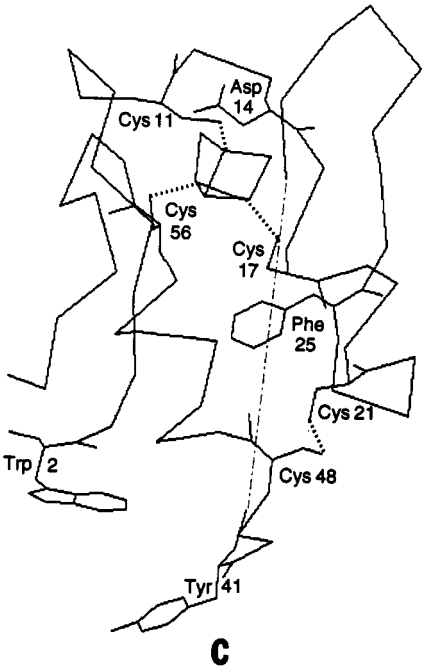

FIGURE 1: (A) Alignment of amino acid sequences for ferredoxins from *Pf* Fd, *Tl* Fd, and *Dg* Fd. Numbering is based upon *Pf* Fd as it is the longest protein. Cysteines are identified by Roman numerals to allow easier comparison of equivalent residues. (B) Conformation of cysteines around the 3Fe-4S cluster based upon *Dg* Fd X-ray diffraction structure (Kissinger et al., 1988); residues numbers are for *Pf* Fd. (C) α-Carbon chain for the proposed structure of *Pf* Fd based upon the coordinates of the *Dg* Fd. Aromatic residues, cysteines, and Asp-14 are identified for comparison to text discussion. The dashed light line indicates the variable loop region, residues ca. 34–46.

dimensional NMR identification of the signal of individual cysteines has verified the predicted temperature dependence patterns (Banci et al., 1991b; Bertini et al., 1990, 1991a,b, 1992a; Busse et al., 1991; Cowan & Sola, 1990) and for several proteins has identified the sequence origin of the valence state differentiated irons (Dugad et al., 1990; Skjeldal et al., 1991; Nettesheim et al., 1992; Bertini et al., 1992b).

In contrast, 3Fe clusters have been studied by NMR primarily in proteins that possess both the 3Fe and 4Fe clusters so it has not even been possible to associate all of the contact-shifted cysteinyl residues to the respective clusters (Nagayama et al., 1986; Cheng et al., 1990). In order to elucidate the ^{1}H NMR spectral parameters that reflect electronic/magnetic properties common to, and perhaps diagnostic for, 3Fe systems, we have investigated the NMR spectra of the ferredoxin (Fd)[1] from two hyperthermophilic archae (formerly archaebacteria), *Pyrococcus furiosus* (*Pf*) and *Thermococcus litoralis* (*Tl*), organisms that grow optimally near or at 100 °C (Fiala & Stetter, 1986; Neuner et al., 1990). Both proteins are comprised of about 65 residues (Figure 1A) and contain a single 4Fe cluster which readily converts to stable 3Fe forms (Conover et al., 1990a).[2] They exhibit extensive sequence homology to the 3Fe Fd from the mesophilic bacterium *Desulfovibro gigas* (*Dg*), for which an X-ray crystal structure (Figure 1B,C) has been reported (Kissinger et al., 1988, 1989), and computer modeling has predicted strong structural homology to *Dg* Fd.[2] However, these hyperthermophilic proteins are stable to significant denaturation over 12 h at 95 °C (Aono et al., 1989)[2] and, in physiological electron transfer reactions to hydrogenase, appear to function efficiently only above 80 °C (Bryant & Adams, 1989; Adams, 1992). While *Tl* 4Fe Fd has the usual 4 cysteinyl ligation to the cluster,[2] *Pf* 4Fe Fd has one residue replaced by an aspartyl group which accounts for the ease of removal of one Fe, the anomalous resonance Raman properties of the 4Fe cluster (Conover et al., 1990a), the ability of the 4Fe cluster to bind exogenous ligands (Conover et al., 1991), and the ease with which other metal ions (M) can be accommodated to generate mixed metal [MFe_3S_4]-type clusters (Conover et al., 1990b). A recent ENDOR study concluded hydroxide is likely to furnish the fourth ligand in the reduced 4Fe cluster of the *Pf* protein (Park et al., 1991).

In this initial NMR study, we have addressed the following questions: (1) Do these hyperthermophilic 3Fe Fds exhibit a protein folding pattern similar to that of the mesophilic *Dg* 3Fe Fd, as predicted by computer modeling? Can the β-methylene signals for the coordinated cysteines be located? Do the contact shifts for the cysteines reflect a characteristic pattern that can be interpreted in terms of the electronic/magnetic properties of the cluster? Do the iron within the oxidized cluster exhibit the asymmetry that can form the basis for the "special pair" in the reduced cluster? Lastly, can the signals from coordinated cysteines be sequence-specifically

[1] Abbreviations: NMR, nuclear magnetic resonance; EPR, electron paramagnetic resonance; DSS, 2,2'-dimethyl-2-silapentane-5-sulfonate; ppm, parts per million; NOE, nuclear Overhauser effect; NOESY, nuclear Overhauser effect spectroscopy; COSY, correlation spectroscopy; DQF-COSY, double-quantum-filtered correlation spectroscopy; Fd, ferredoxin, HiPiP, high-potential iron protein; *Dg*, *Desulfovibro gigas*; *Pf*, *Pyrococcus furiosus*; *Tl*, *Thermococcus litoralis*.

[2] J. B. Howard, J.-B. Park, Z. H. Zhai, and M. W. W. Adams, manuscript in preparation.

assigned to assess the structural basis of the asymmetry of the electronic structure?

MATERIALS AND METHODS

Proteins. *P. furiosus* (*Pf*) cells were grown (Bryant & Adams, 1989), and its ferredoxin (Fd) was isolated and purified (Aono et al., 1989) and converted to the 3Fe form (Conover et al., 1990a) as described previously. Growth of *T. litoralis* (*Tl*) cells[3] and the characterization of its ferredoxins will be described elsewhere. The NMR samples were prepared by exchanging the ^1H_2O solution with a 25 mM sodium phosphate ^2H_2O buffer in an Amicon ultrafiltration device using a YM3 membrane at pH 7.8–7.9. The NMR spectra parameters were found to be pH independent within ±0.5 pH unit of these values (data not shown).

NMR Spectroscopy. All NMR spectra were acquired on a General Electric Ω500 NMR spectrometer operating at 500-MHz proton frequency. One-dimensional spectra were recorded with either a slow repetition time (3 s) using presaturation for water suppression or with a fast repetition time (100 ms) using a super-WEFT pulse sequence (Inubushi & Becker, 1983) with a 40–60 ms relaxation delay between the 180° and 90° pulse sequence for water suppression. Spin-lattice relaxation times (T_1) were measured using an inversion–recovery sequence; repetition times were set at 5 times the T_1 relaxation time of the peaks of interest. The relaxation times were determined using a three-parameter fit of the data for resolved resonances. T_1s for unresolved peaks were estimated by the inversion null point for fast relaxing resonances under conditions where nearby slow relaxing signals are strongly suppressed. One-dimensional NOE experiments were performed using a SUPER-WEFT pulse sequence; repetition times of 100 ms were used with a relaxation delay of 40–60 ms. The resonance under study was irradiated for 95% of the relaxation delay time. NOE difference traces were acquired by interleaving a block of scans with saturation on-resonance with an equal number of blocks with off-resonance saturation and taking the difference between these two sets of scans. Sweep widths of 25 000 Hz and 30 000 Hz were used for *Pf* and *Tl* Fd, respectively. Line widths for resolved peaks were determined by fitting the entire hyperfine region (30 ppm to 7.0 ppm) to a series of Lorentzian lines. For unresolved peaks of interest, the line width was estimated from the lineshape of the nuclear Overhauser effect, NOE, response in a 1D NOE difference trace. The steady-state NOE from peak j to peak i is given by (Neuhaus & Williamson, 1989)

$$\eta_{j\rightarrow i} = \sigma_{ij} T_{1i} \tag{2}$$

where σ_{ij} is the cross-relaxation rate given by

$$\sigma_{ij} = 0.1\gamma^{4\hbar 2} r_{ij}^{-6} \tau_c \tag{3}$$

with r_{ij} the interproton distance and τ_c the reorientation time of the ij vector, which can be assumed to be the rotational correlation time of the protein, τ_r. This, in turn, can be estimated from the Stokes–Einstein equation

$$\tau_r = 4\pi a^3 \zeta / 3kT \tag{4}$$

where a is the protein radius and ζ is the solvent viscosity. For a globular protein of $M_r \sim 7000$, as in the case for *Pf* and *Tl* Fd, eq 3 yields $\tau_r \sim 3$ ns at 30 °C in ^2H_2O.

Two-dimensional NMR experiments were performed either as fast repetition rate experiments to study the hyperfine shifted resonances (Busse et al., 1991; La Mar & Ropp, 1993) or as slow repetition rate, high-resolution experiments. MCOSY experiments (Bax, 1982) were collected as n-type spectra with sweep widths of 25 000 Hz and 30 000 Hz used for *Pf* Fd and *Tl* Fd, respectively. The data consisted of 1024 t_2 points and 256 t_1 blocks with a pulse repetition time of 50 ms. The data were processed using 0°-shifted sine-squared window functions over 256 points in both dimensions, and zero-filled to 1024 × 1024 final size. Because of the rapid decay of magnetization, the sensitivity in COSY and NOESY (see below) experiments was improved by using only one-quarter of the collected data points in the t_2 direction (Busse et al., 1991; La Mar & de Ropp, 1993). NOESY data were collected over the same bandwidths with TPPI phase-sensitive detection (Marion & Wüthrich, 1983), using 1024 t_2 points and 256 t_1 blocks; the mixing time was 10 ms and the repetition time was 50 ms. The data were processed using 60°-shifted sine-squared windows over 256 points in both dimensions. The data were baseline-straightened after the first FT using a fourth-degree polynomial function. High-resolution NOESY and DQF-COSY experiments were collected as 512 t_1 blocks of 2048 t_2 points over 7000 Hz for both proteins. Pure phase spectra were collected using TPPI with a mixing time of 250 ms and were processed using 60°-shifted sine-squared windows in both dimensions. DQF-COSY data were processed using 0°-shifted sine-squared windows in both dimensions. All 2D data processing was performed using the FELIX program by Hare Research Inc. Chemical shifts are reported in parts per million referenced to 2,2-dimethyl-2-sila-5-pentanesulfonate (DSS) via the residual solvent line.

RESULTS

The oxidized 3Fe forms of *Pf* Fd and *Tl* Fd were used throughout the following experiments.

The complete 500-MHz ^1H NMR spectra in ^2H_2O at 30 °C under nonsaturating conditions (pulse repetition rate 0.33 s^{-1}) for these proteins are illustrated in Figure 2A,D. The resonances of interest are labeled by lowercase letters. Spectra were also collected under rapid pulsing condition (pulse repetition rate 10 s^{-1}) that emphasize fast-relaxing proton signals and significantly suppress the slowly relaxing envelope, and these are given in Figure 2B,E. The super WEFT (Inubushi & Becker, 1983) trace for *Pf* Fd shown in Figure 2C suppresses signals with $T_1 > 30$ ms and allows detection of two severely relaxed proton peaks h and p. The resolved portions in Figure 2A,D consist of a single slowly relaxing upfield methyl, numerous slowly relaxing resonances in the aromatic window 6–7 ppm, and 6–7 broad low-field signals in the 8–30 ppm region that clearly experience contact shifts and significant paramagnetic relaxation. Signal intensities were determined by peak integration under conditions where neither the signal of interest nor the reference signal is saturated. The upfield three-proton methyl peak z (confirmed by 2D; see below) served as intensity reference for slowly relaxing protons, while the narrowest low-field Cys single proton peak (confirmed by 1D NOEs; see below) served as reference for rapidly relaxed protons. The chemical shifts, line widths, and nonselective T_1 values for resolved signals at 30 °C are listed in Table I. Because *Pf* Fd is more readily obtained and has been more extensively characterized (Aono et al., 1989; Bryant & Adams, 1989; Connover et al., 1990a; 1991; Park et al., 1991), we focused primarily on the *Pf* Fd; less extensive studies were carried out with the more recently characterized *Tl* Fd.[2,3]

Assignment of Aromatic Residues. *Pf* Fd has three aromatic residues, Trp 2, Phe 25, and Tyr 46.[2] Portions of

[3] S. Makund, and M. W. W. Adams, manuscript in preparation.

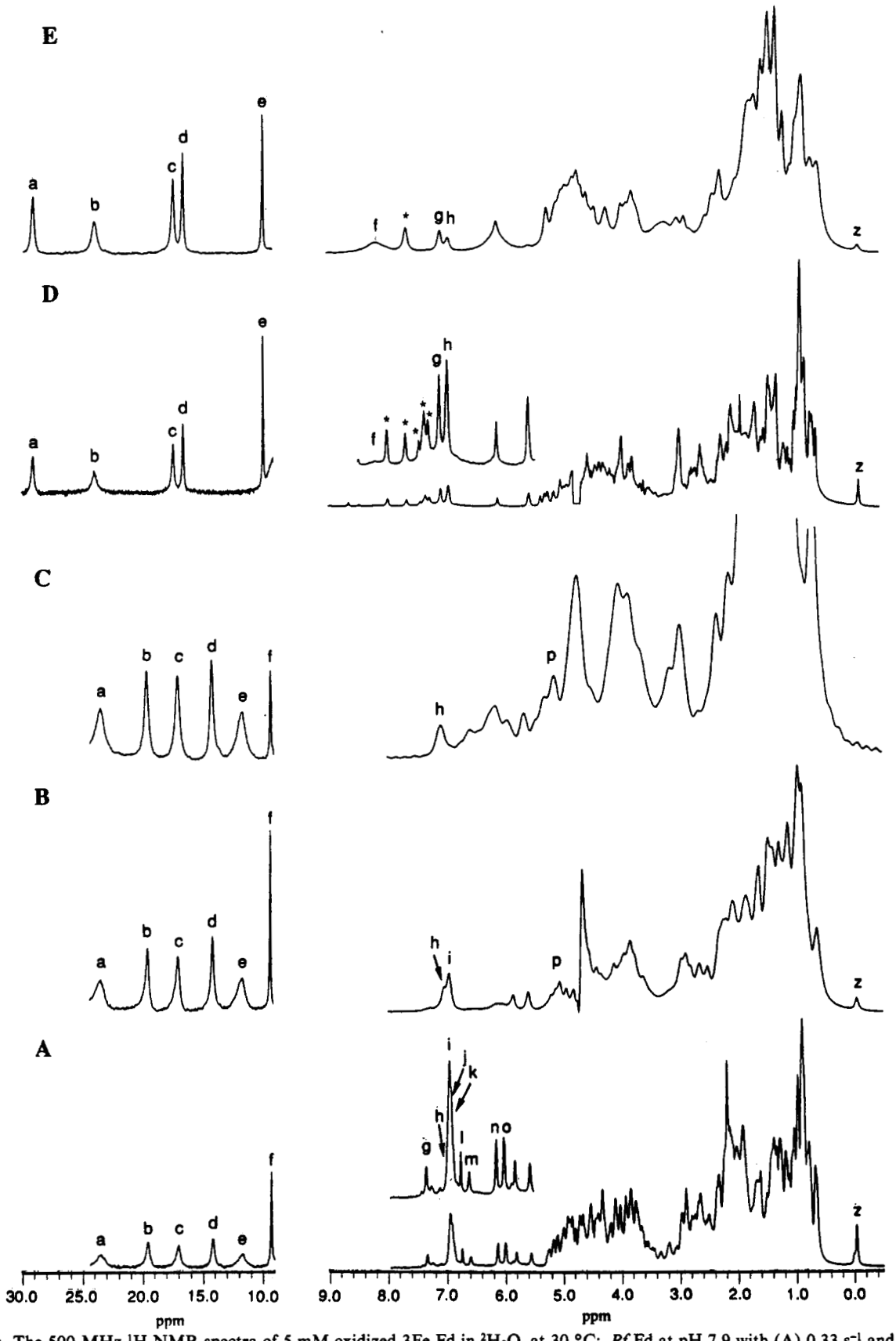

FIGURE 2: The 500-MHz ^1H NMR spectra of 5 mM oxidized 3Fe Fd in ^2H_2O, at 30 °C: *Pf* Fd at pH 7.9 with (A) 0.33 s^{-1} and (B) 10 s^{-1} pulse repetition rates and (C) Super-WEFT spectrum revealing peaks h and p; *Tl* Fd at pH 7.8, with (D) 0.33 s^{-1} and (E) 10 s^{-1} pulse repetition rates. The repetition rate emphasizes fast relaxing peaks, particularly within the diamagnetic envelope. The resonance of interest in this report are labeled with lowercase letters.

its DQF-COSY spectrum, illustrated in Figure 3, reveal that the upfield methyl peak z is part of a valine (Figure 3A), while peaks n and o arise from the 2,6-H and 3,5-H of Tyr 46 (Figure 3B). The protons of the six-membered ring of Trp 2 are located in the DQF-COSY map by two cross peaks at 6.62 (m), 6.91 (j), and 7.35 (g) ppm (Figure 3B). The fourth signal is under the broad composite at ~6.9 ppm. The expected COSY cross-peak to that resonance is too close to

Table I: ^{1}H NMR Spectral Parameters for Coordinated Cysteinyl Protons in the 3Fe Forms of *Pf* Fd and *Tl* Fd

protein	Cys[a]	peak[b]	assignment[c]	T_1[d]	line width[e]	δ_{obs}[f]	δ_{con}[g]	$\langle\delta_{con}(C_\beta H)\rangle$[h]	$\delta_{con}(C_\beta H)/\delta_{con}(C_\beta H')$
Pf Fd	A	d	$C_\beta H$	10.6	140	14.27	11.3	7.3	3.5
		p	$C_\beta H'$	<5	~160	5.22	3.2		
		f	$C_\alpha H$	39	48	9.37	4.7		
Pf Fd	B	b	$C_\beta H$	8.7	180	19.73	16.7	15.4	1.2
		c	$C_\beta H'$	2.9	210	17.14	14.1		
		h	$C_\alpha H$	<5	~170	7.09	2.7		
Pf Fd	C	a	$C_\beta H'$	5.0	375	23.65	20.7	14.8	0.43
		e	$C_\beta H$	10.0	300	11.82	8.8		
		s	$C_\alpha H$		~120	3.94	–0.6		
Tl Fd	A	d	$C_\beta H$	9.1	71	16.59	13.6	9.4	2.7
		f	$C_\beta H'$	~5	~190	8.12	5.1		
		e	$C_\alpha H$	15.5	37	9.88	5.2		
Tl Fd	B	c	$C_\beta H'$	5.2	102	17.41	14.4	8.2	0.13
		i	$C_\beta H$		~80	4.85	1.9		
		j	$C_\alpha H$		~50	3.76	–0.9		
Tl Fd	C	a	$C_\beta H$	5.5	120	29.15	26.2	23.6	1.2
		b	$C_\beta H'$	1.7	255	23.96	21.0		

[a] Cys designation is C (for Curie-like temperature dependence) and A (for near aromatic, i.e., conserved Phe). [b] Peak labels as given in Figures 2–5. [c] $C_\beta H$ and $C_\beta H'$ designated the Cys β-methylene proton further from and closer to the iron, respectively, as reflected in their T_1 values. [d] T_1 values are in milliseconds, with uncertainty ±20%; values preceded by ~ are determined from null point during an inversion recovery experiment under sufficiently rapid pulsing conditions to suppress slowly relaxing protons. [e] Line width values are in hertz at 500 MHz, with uncertainty of ±20%. [f] With observed shift, relative to DSS, given in parts per million. [g] $\delta_{con} = \delta_{obs} - \delta_{dia}$, with δ_{dia} in the shift in a diamagnetic complex, $\delta_{dia}(C_\beta H) = 2.0$, $\delta_{dia}(C_\alpha H) = 4.5$ ppm. [h] $\langle\delta_{con}(C_\beta H)\rangle = [\delta_{con}(C_\beta H) + \delta_{con}(C_\beta H')]$.

the diagonal to detect. The Trp 2 2-H signal, l, is a sharp singlet in ^2H_2O at 6.76 ppm. The composite signal, i, with an approximate five-proton intensity at 6.94 ppm, fails to exhibit any COSY cross-peaks and, hence, must arise from the essentially degenerate protons of Phe 25. This accounts for all of the signals from the three aromatic side chains. The signal h arises from a coordinated Cys $C_\alpha H$ (see below). The remainder of the narrow weak signals in the region 6–10 ppm arise from slowly exchanging labile protons which are not relevant at this time. The Trp 2 and Tyr 46 signals all exhibit very long T_1s, >2 s, indicating locations remote from the cluster. The five-proton Phe 25 composite exhibits a shorter effective $T_1 \sim 100$ ms, indicating a position close to the cluster. The NOESY spectrum for the 0–10 ppm window in Figure 3C exhibits the expected intraresidue cross-peaks for the above-identified aromatic and valine side chain (Figure 3C). Intense cross-peaks between the upfield-shifted valine methyl peak z and the Phe 25 aromatic ring composite dictate close proximity of these two side chains (Figure 3D). Strong cross-peaks are also observed between the Trp 2 and Tyr 46 aromatic chain protons (Figure 3E). Hence, the sequence positions 2 and 46 form a close tertiary contact, as predicted by computer modeling based on the sequence.[2] The remainder of the aromatic dipolar contacts are to as yet unassigned residues.

In contrast, to *Pf* Fd, *Tl* Fd possesses a single aromatic residue, Phe 24.[2] The two resolved peaks at 6.62 (g) and 6.47 ppm (h), with relative areas 2:3, yield a DQF-COSY cross-peak identifying them as the 2,6-H and 3,5-H/4-H composite of Phe 24 (supplementary material). The upfield-resolved methyl peak z exhibits cross-peaks diagnostic of a Val. The NOESY spectrum displays intense cross-peaks between the Val methyl peak z and the Phe 24 3,5-H/4-H composite (not shown; see supplementary material). The peaks marked with asterisks in Figure 2D arise from incompletely exchanged labile protons. Having accounted for all the aromatic side chain signals for nonlabile protons in the low-field side of 5.5 ppm, and failing to observe any intensity decrease in ^2H_2O over a period of two years during which other obvious labile proton signals slowly disappeared, we conclude that the remainder of the signals in the low-field spectral window must originate from the cysteines coordinated to the cluster; 1D NOEs confirm this (see below). The chemical shifts for the assigned noncoordinated residues are listed in Table II.

Location of Cysteinyl Resonances. The line width and T_1s of the likely cysteinyl resonances for *Pf* Fd and *Tl* Fd are listed in Table I. Although the pattern of chemical shifts and T_1s in the 8–30 ppm are similar in the two proteins, *Pf* Fd exhibits ~50% greater widths for many of the resonances as compared to *Tl* Fd. Therefore, *Pf* Fd failed to exhibit COSY cross-peaks for any of the low-field hyperfine shifted resonances, even under rapid pulsing conditions optimized for detecting broad resonances (not shown). However, the NOESY spectrum collected under rapidly pulsing conditions contained cross-peaks between resonances a and e, b and c, and d and f (Figure 4C), indicating that these resonances can be paired into three sets for the three coordinated cysteines. Although the cross-peak intensity cannot be interpreted in terms of distance, the 1D NOE of ~ –6% for peak a to e and ~ –5% for peak c to b (supplementary material) yield internuclear distances of ~1.8 Å using eqs 2 and 3. This establishes two of the three pairs of β-methylene protons for the coordinated cysteines. The ~ –1.5% 1D NOE from peak d to f (Figure 4B), together with the $T_1 = 39$ ms for f, however, yields $r_{df} \sim 2.7$ Å, indicating that d and f are not geminal but vicinal partners. The assignment of peak f to $C_\alpha H$ rather than $C_\beta H$ of a cysteine is reflected in its smaller line width and longer T_1 than the other resolved resonances. Consistent with this conclusion, the 1D NOE difference trace upon saturating peak d yields a ~ –3% NOE to a broad, rapidly relaxed resonance p ($T_1 \sim 5$ ms; line width 160 Hz) in the diamagnetic envelope at 5.22 ppm (Figure 4B); this resonance p is assigned to the geminal partner to peak d for the $C_\beta H_2$ of the third coordinated cysteine, with peak f as the $C_\alpha H$. The likely $C_\alpha H$ peaks for the other two cysteine were identified by detecting weak 1D NOEs (~ –1%) to unresolved broad (>100 Hz) resonances.

For *Tl* Fd, the contact-shifted low-field lines yield MCOSY cross-peaks for the two narrowest lines c and d, with the obvious geminal partners for these protons, peaks i and f, respectively, located in the diamagnetic envelope (Figure 5D). The geminal nature of these spin-coupled protons is confirmed by ~ 3%

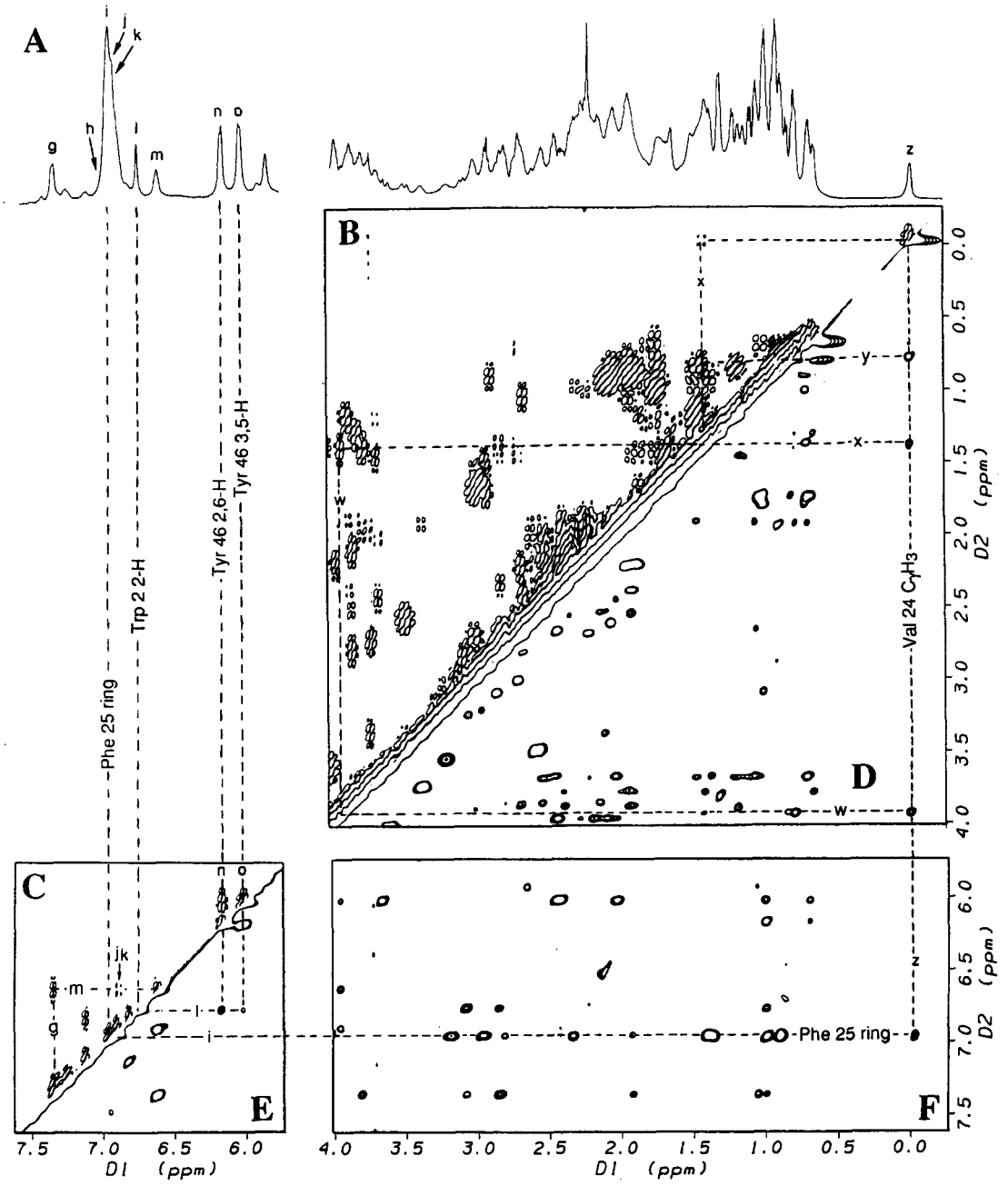

FIGURE 3: (A) The 500-MHz ^1H NMR reference trace for the resolved diamagnetic region of 5 mM *Pf* Fd in ^2H_2O, pH 7.9, at 30 °C. The labeling of the resonances is the same as in Figure 2A. Split-diagonal sections of the (B) upfield and (C) low-field region DQF-COSY map exhibit the bond correlation for Trp 2, Tyr 46, and Val 24; the phenyl resonances for Phe 25 are essentially degenerate. Split-diagonal portions of the NOESY map (mixing time 150 ms) exhibiting the dipolar show correlation (D) within the upfield Val 24 peaks, (E) among the aromatic side chain protons of Trp 2 and Tyr 46, and (F) between portions of Phe 25 and Val 24.

to ~6% NOEs to these same unresolved resonance (Figure 5C; supplementary material). The two lowest field lines failed to exhibit any MCOSY cross-peaks likely because of their greater line widths. However, the 1D NOE difference trace upon saturating peak b yields a NOE to peak a (Figure 5C), indicating that a and b are the β-methylene protons of the third cysteine coordinated to the cluster. The 1D NOE difference trace upon saturating peak d yields a NOE not only to its geminal partner, f, at 8.12 ppm detected in the COSY spectrum (Figure 5D), but also to the narrower contact shifted resonance e. The smaller line width and longer T_1 for peak e dictates that it originates from the $C_\alpha H$ of the cysteine with peaks d and f as $C_\beta Hs$.

Temperature Dependence of Contact Shifts. The chemical shifts for the assigned cysteinyl resonances of *Pf* Fd and *Tl* Fd are plotted as a function of reciprocal temperature (Curie plot) in Figure 6. For each protein, the peaks of only one cysteine exhibit Curie-like behavior (contact shifts increase with decreasing temperature), and we label this as Cys C (for Curie-like); the resonances for the other two cysteins are labeled Cys A and Cys B, and they exhibit anti-Curie behavior (shifts increase with increasing temperature). Therefore, there is clearly a common magnetic asymmetry among the 3Fe of the cluster in each of these proteins.

For *Pf* Fd, the line widths of several resonances (in particular a, b, and e) exhibit a much stronger temperature dependence than the others in this protein or any of the line widths for *Tl* Fd. These lines become broader as the temperature is lowered and at 20 °C split into two sets of resonances of comparable areas as illustrated in Figure 7. The splitting is greatest for the resonances of Cys C, less for Cys B, and not detectable for Cys A. Hence, *Pf* Fd^{ox} can exist in two comparably

Table II: ^{1}H NMR Spectral Parameters for Assigned Side Chain Resonance in the 3Fe Forms of *Pf* Fd and *Tl* Fd

protein	residue	peak label	assignment	T_1[a]	δ_{obs}[b]
Pf Fd	Trp2	j	6-H	>2	6.91
		k	7-H		6.91
		g	4-H	≥2	7.35
		m	5-H	~2	6.62
		l	2-H	>2	6.76
Pf Fd	Phe25	i	4-H, 2,6-H, 3,5-H	0.1	6.94
Pf Fd	Tyr46	n	2,6-H	>3	6.17
		o	3,5-H	>3	6.02
Pf Fd	Val24	z	$C_\gamma H_3$	~3	−0.01
		y	$C_\gamma H_3'$		0.79
		x	$C_\beta H$		1.43
		w	$C_\alpha H$		3.94
Tl Fd	Phe24	g	2,6-H	0.09	6.62
		h	3,5-H, 4-H	0.12	6.47
Tl Fd	Val23	z	$C_\gamma H_3$		−0.11
		y	$C_\gamma H_3'$		0.66
		x	$C_\beta H$		1.31
		w	$C_\alpha H$		3.86

[a] T_1, in seconds, ± 20%. [b] Shift is in parts per million from DSS at 30 °C in ^2H_2O, pH 7.0.

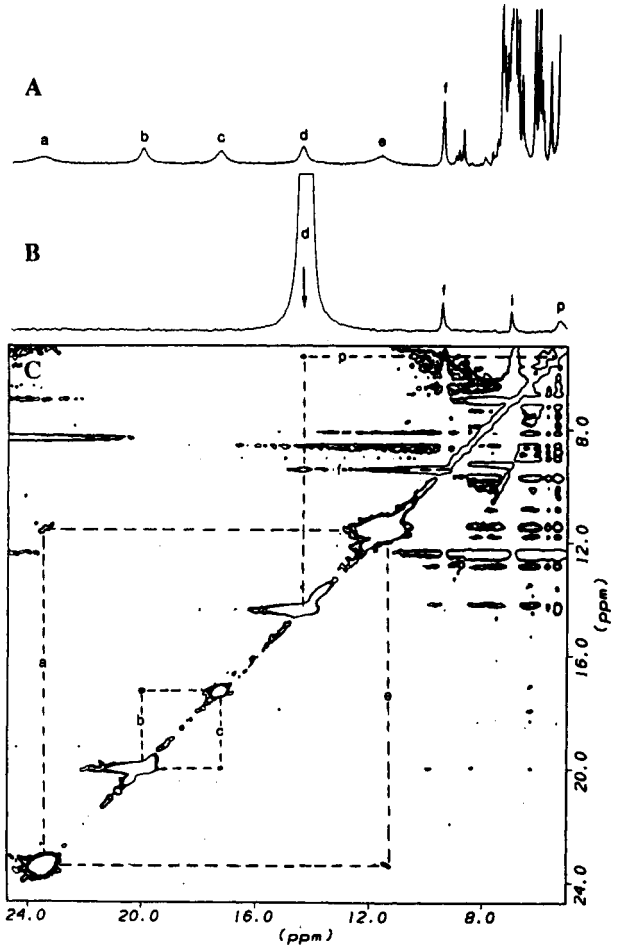

FIGURE 4: (A) Low-field portion of the 500-MHz ^{1}H NMR spectra of 5 mM *Pf* Fd in ^2H_2O, pH 7.9 at 30 °C, with resonances labeled as in Figure 2A. (B) 1D NOE difference trace obtained upon saturating peak d; note the ~ −5% NOE to the broad and rapidly relaxing peak labeled p, and to the narrower resolved resonance f. (C) NOESY spectrum collected with 10-ms mixing time under rapid pulse repetition (20 s^{-1}) to focus on cross-peaks among strongly relaxed protons. The region to the high field of 7 ppm is obscured by t_1 ridges and artifacts resulting from the rapid pulse repetition rate needed to obtain reasonable sensitivity for the cross-peak.

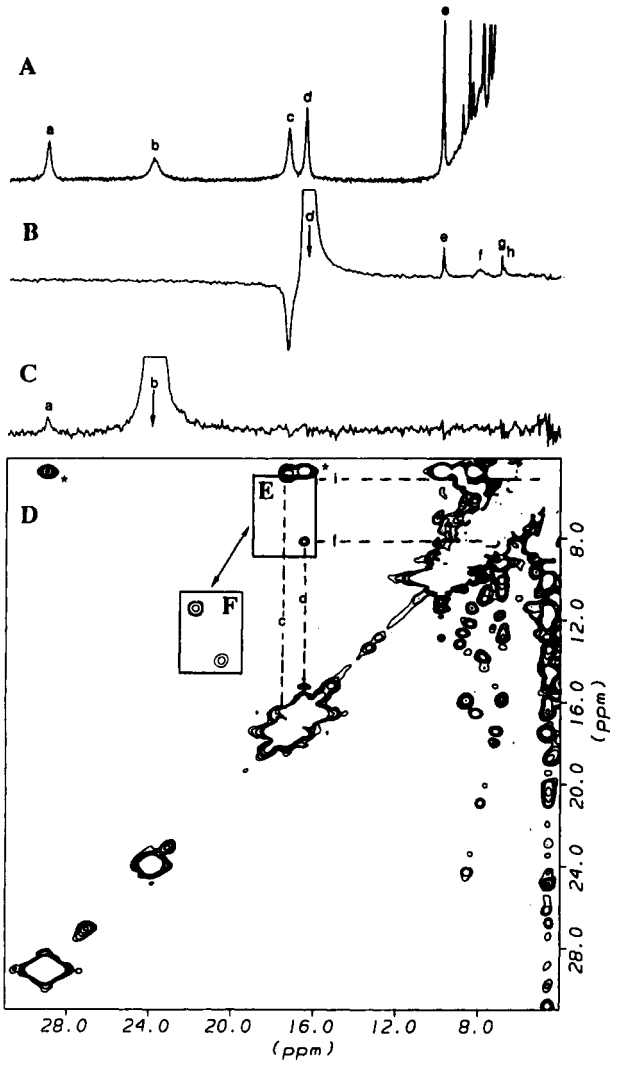

FIGURE 5: (A) Resolved portion of the 500-MHz ^{1}H NMR spectra of *Tl* Fd in ^2H_2O, pH 7.8, at 30 °C with peaks labeled as in Figure 3C. (B) 1D NOE difference trace obtained upon saturating peak d; note the NOE to the narrow contact shifted signal e, as well as to the broad, rapidly relaxed resonance labeled f. (C) 1D NOE difference trace obtained upon saturating peak b; note the NOE to peak a, which identifies it as its geminal partner. (D) Low-field portion of the magnitude COSY spectra collected under rapid pulse repetition (15 s^{-1}) conditions showing cross-peaks detected for the narrow low-field peaks c and d. The upfield portion of the map is obscured by artifacts resulting from the rapid pulsing rate needed to obtain reasonable sensitivity for the cross-peak. The cross-peak between peaks c and i overlaps a strong solvent ridge at 30 °C (E); however, at 45 °C the solvent line and peak c are sufficiently resolved to reveal the cross-peak (F).

populated interconvertible forms for which the heterogeneity influences the environment primarily for Cys C, less for Cys B, and inconsequentially for Cys A. The line width of peak b at coalescence at 20 °C indicates an interconversion rate of ~6×10^3 s^{-1} (Sandström, 1982). The exchange contribution to the chemical shift in the temperature range 5–20 °C does not allow the determination of the intrinsic temperature dependence of the peaks from the resolved components in the absence of exchange.

Relaxation Properties of Cysteinyl Protons. The T_1s have been determined for the three pairs of cysteinyl β-protons in *Pf* Fd and five of the six comparable protons in *Tl* Fd; one of the *Tl* Fd protons resonates too near (5.22 ppm) the residual water solvent peak to allow more than a crude estimate of ~10 ms for this proton. Because there is a good correlation between shorter T_1 and larger line width for the cysteinyl β-protons of *Tl* Fd, either parameter can be used to identify the more strongly relaxed proton in each β-methylene pair and, hence, which proton is closer to the coordinated iron

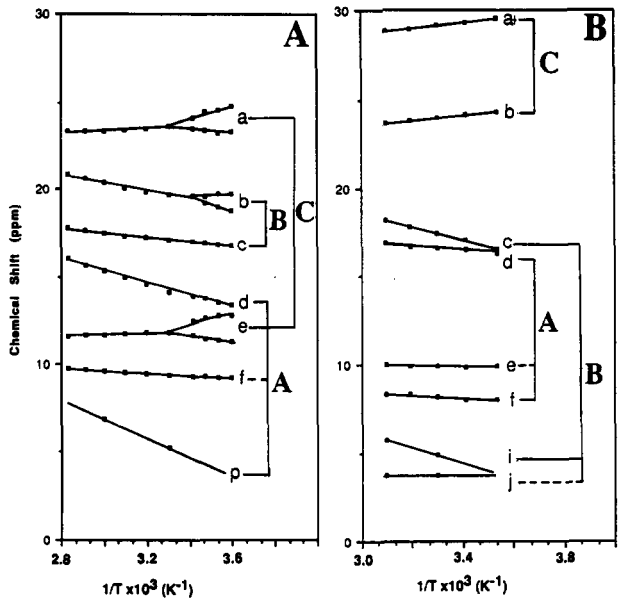

FIGURE 6: Plot of observed shift, relative to DSS, versus reciprocal absolute temperature (Curie plot) for the identified cysteinyl resonance for (A) *Pf* Fd and (B) *Tl* Fd. The individual resonances are labeled as in Figures 2, 3, and 4 and Table I; the cysteines are labeled A for that close to the invariant phenylalanine and C for that exhibiting Curie-like behavior. The remaining cysteine is labeled Cys B.

(Busse et al., 1991). However, exchange processes involving alternate local conformations lead to line broadening of some resonances in *Pf* Fd and preclude the use of line width for consideration of proton orientation. A comparison of the pairs of cystein β-protons reveals an interesting difference between the magnetic properties of the [3Fe-4S] cluster in the two proteins. For the Cys A proton pair (defined as the cysteine nearest the aromatic ring of the conserved phenylalanine in each protein; see below), the proton with the significantly shorter T_1 and therefore, nearest the iron, has the smaller contact shift in both proteins. In contrast, the protons of Cys C (the Curie-dependent cysteinyl resonances) differ in the two proteins. Namely, the *Pf* Fd, the Cys C proton closer to the iron has the larger contact shift while in *Tl* Fd the closer proton has the smaller shift. A similar difference is also found for the remaining cysteine, designated Cys B. That is, in *Pf* Fd the Cys B proton closer to the iron has the smaller contact shift while the converse is seen for Cys B protons in *Tl* Fd. Thus, the orientation of the cysteines in the two protein is such that only one of the cysteins exhibits a larger contact shift for the proton closer to the iron (Cys C in *Pf* Fd and Cys B in *Tl* Fd), yet the magnetic properties of the coordinated iron are *not* reflected in the common orientation, namely Cys C has Curie temperature dependence while Cys B has anti-Curie dependence.

DISCUSSION

Tertiary Structure. Computer modeling of the hyperthermophilic proteins, *Pf* Fd and *Tl* Fd, based on the sequences and the crystal structure in *Dg* Fd, has already predicted very similar folding patterns for them.[2] The strongest support for extensive structural homology among these proteins and the structurally characterized *Dg* Fd is the conservation not only the Cys positions I, III, and IV in Figure 1C that coordinate the 3Fe cluster (Figure 1B) but also of the two Cys positions V and VI that form the disulfide bond in *Dg* Fd (Figure 1A). Accordingly, it has been proposed that these two cysteines

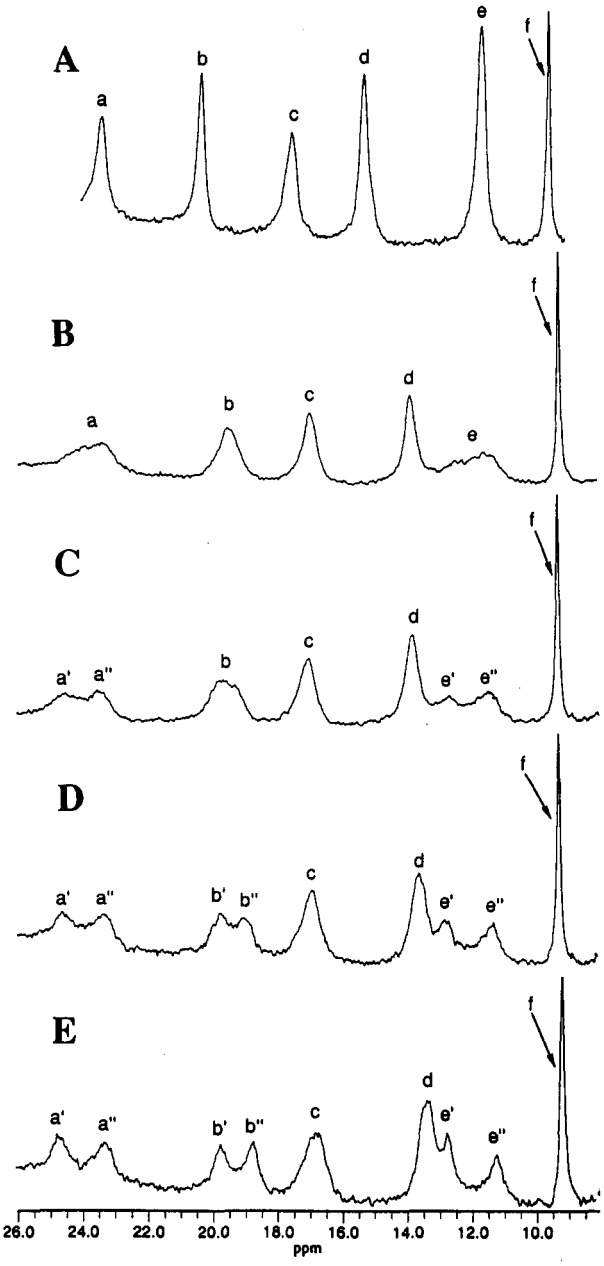

FIGURE 7: The 500-MHz ^{1}H NMR spectra of 3 mM *Pf* Fd in ^2H_2O, pH 7.9, as a function of temperature: (A) 50 °C, (B) 20 °C, (C) 15 °C, (D) 10 °C, (E) 5 °C. Note the splitting of resonance from peaks a, b, and e (the split components are labeled by primes and double-primes).

form a disulfide bond in both of the hyperthermophilic Fds.[2] *Dg* Fd additionally possesses Cys II which does not participate in coordination to the cluster even in the 4Fe analog, and it has been proposed that this cysteine is chemically modified (Kissinger et al., 1989). In *Pf* Fd the position homologous to Cys II in *Dg* Fd is occupied by Asp 14.[2] Although *Tl* Fd has Cys II, the strong similarity of the cysteine contact shift pattern to both *Dg* Fd and *Pf* Fd support the conclusions from modeling that it is not coordinated to an iron in the 3Fe form of the protein.

The limited ^{1}H NMR assignments available do not allow a quantitative comparison of the folding pattern of *Pf* Fd and *Tl* Fd with the crystallographically characterized *Dg* Fd (Kissinger et al., 1988, 1989). However, several of the tertiary contacts identified in this work provide direct support for the predicted structural homology to *Dg* Fd.[2] The crystal coordinates to *Dg* Fd predict only one strongly upfield ring

current shifted methyl, that of Val 21 interacting with the aromatic ring of Phe 22 on a β strand (Kissinger et al., 1988, 1989; E. T. Adman, private communication); a methyl peak at ~0 ppm with the correct ring current shift is observed for *Dg* Fd (Moura et al., 1977). The observation of essentially the same upfield ring current shift for a valine methyl (Val 24 in *Pf* Fd, Val 23 in *Tl* Fd) interacting with the conserved sole Phe (Phe 25 in *Pf* Fd, Phe 24 in *Tl* Fd) in the hyperthermophilic Fds indicates very similar interaction on a conserved β strand. One important conserved structural feature detected only in *Pf* Fd is the interaction between the side chains of Trp 2 and Tyr 46 (Figure 3C). This indicates that the amino terminus of the protein is near a loop leading into the presumed disulfide bridge (Figure 1A); such an interaction has been predicted by a model of *Pf* Fd.[2]

The remaining structural feature common to these 3Fe Fd is the position of the invariant Phe side chain in relation to the cluster, and in particular, to the buried Cys III (see Figure 1C). The crystal coordinates of *Dg* Fd (Kissinger et al., 1988, 1989),[4] as well as the computer modeling in *Pf* Fd and *Tl* Fd,[2] place the aromatic ring close to C_βHs of only the buried Cys III. In *Dg* Fd, the distance between the Cys 14 C_βH and the Phe 22 ring is 3.5 Å, while the distance between the ring and the nearest iron is 5.9 Å. From this one would expect a detectable Cys II C_β to ring NOE and significant paramagnetic relaxation effects for the invariant phenylalanine ring protons. Saturation of the C_βH of only one cysteine (Cys A) in each of *Pf* Fd and *Tl* Fd yields an NOE to the invariant aromatic side chain protons (Figures 4C and 5D). The T_1 for the phenylalanine side chain peaks is ~100 ms in *Pf* Fd and *Tl* Fd^{ox}, which confirms the predicted proximity of the aromatic ring to the iron cluster. Similar NMR data have not been reported for *Dg* Fd to date. This latter interaction between the conserved Phe and Cys A not only confirms that the folding pattern is conserved among these 3Fe Fds but also provides the sequence-specific assignment for Cys A (labeled A for near aromatic) as Cys III. Likewise, Cys A exhibits strong and similar anti-Curie behavior (Figure 7) in both of the hyperthermophilic Fds.

Electronic/Magnetic Properties of the Oxidized 3Fe Cluster. Both of the hyperthermophilic Fds exhibit Curie-like behavior for both C_βHs of only a single cysteine (labeled Cys C in Table I), with the C_βHs of the other two, Cys A and Cys B, exhibiting anti-Curie behavior (Figure 6). Therefore, in spite of the fact that the magnetic and electronic properties of the 3Fe cluster are thought to arise from the coupling of three apparently identical high-spin ferric ions (Huynh et al., 1980; Emptage et al., 1980), the NMR detectable couplings must result from a 2:1 asymmetry in the iron interactions. This behavior has a ready qualitative rationalization on the basis of the arguments and equations derived to account for the contrasting temperature dependence of the two valence-state differentiated iron pairs in reduced, $S_T = 1/2$, 2Fe plant Fd (Dunham et al., 1970; Banci et al., 1990), oxidized, $S_T = 1/2$, 4Fe HiPiP (Bertini et al., 1991b), and reduced, $S_T = 1/2$, 4Fe Fd (Bertini et al., 1992a). The characteristic temperature dependence is determined by the relative values for the "local" or intermediate spin vectors S_A and S_B, from pairs of iron, $S_A = S_1 + S_2$, $S_B = S_3 + S_4$, that antiferromagnetically couple to yield the final cluster spin ground state, $S_A + S_B = S_T$ (Noodleman, 1988, 1991) (for the 2Fe Fd, the intermediate spin vectors are for the individual iron atoms). At low temperature, the larger local spin S_A aligns with the field (and results in positive spin density or low-field contact shifts for the attached cysteine), while the smaller local spin S_B must align antiparallel to S_A due to the antiferromagnetic coupling, and hence antiparallel to the field (this results in negative spin density or upfield C_βH contact shifts for the coordinated cysteine). At high temperature, the local spins uncouple to both align with the field.

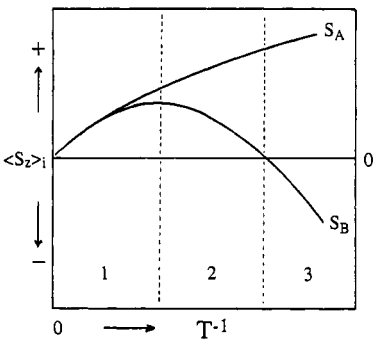

FIGURE 8: Qualitative schematic representation of the temperature dependence with spin magnetization $\langle S_z \rangle$ for the two local or intermediate spin states S_A and S_B, which couple to yield a total cluster spin state S_T. The qualitative behavior shown is that for $|S_A| > |S_B|$. The three regions are (1) high temperature, where both $\langle S_z \rangle_A$ and $\langle S_z \rangle_B$ exhibit Curie-like behavior with the same sign, (2) intermediate temperature where $\langle S_z \rangle_A$ exhibits Curie-like and $\langle S_z \rangle_B$ anti-Curie behavior, both with the same sign, and (3) low temperature where $\langle S_z \rangle_B$ exhibits Curie-like behavior and S_B exhibits Curie-like behavior but with opposite signs from that of $\langle S_z \rangle_A$. The observed temperature dependence for the 3Fe forms of both *Pf* Fd and *Tl* Fd exhibit behavior represented by region 2, with two cysteines exhibiting the behavior by $\langle S_z \rangle_B$ and one showing behavior like $\langle S_z \rangle_A$.

In a plot of $\langle S_z \rangle_i$ (or contact shift) versus reciprocal temperature, this mechanism leads to the general qualitative curves (Dunham, et al., 1970; Banci et al., 1990; Bertini et al., 1991b, 1992a), as shown in Figure 8. At high temperature (left side or region 1 of Figure 8), both $\langle S_z \rangle_A$ and $\langle S_z \rangle_B$ approach Curie behavior with the same sign (low-field) shift. At low temperature (right side or region 3 of Figure 8), the shift for $\langle S_z \rangle_B$ changes sign. In the intermediate temperature region (middle or region 2 of Figure 8) above where the shift for $\langle S_z \rangle_B$ changes sign, $\langle S_z \rangle_A$ exhibits Curie-like behavior and $\langle S_z \rangle_B$ exhibits anti-Curie behavior, both with the same sign. For the reduced 2Fe Fd, $S_A = 5/2$ for the ferric and $S_B = 2$ for the ferrous ion, which leads to the predicted Curie-like and anti-Curie behavior for the cysteines coordinated to the ferric and ferrous ions, respectively (Dunham et al., 1971; Banci et al., 1990; Dugad et al., 1990). For oxidized 4Fe HiPiP, the intermediate spin for the iron pairs are $S_A = 7/2$, for the $2Fe^{2.5+}$ pair and $S_B = 3$ for the $2Fe^{3.0+}$ pair (Noodleman, 1988), with the former exhibiting low-field Curie-like and the latter exhibiting either anti-Curie (region 2 in Figure 8) or high-field "pseudo"-Curie-like (region 3 in Figure 8) behavior (Banci et al., 1991b; Bertini et al., 1991b).

On the basis of a pair-wise coupling to yield a local spin S_B for two of the iron in an oxidized 3Fe cluster (labeled Fe_1 and Fe_2), which couple to a lone F_3 with $S_3 = S_A = 5/2$, the observation of two cysteines with anti-Curie behavior and one cysteine with Curie-like behavior dictates that S_B ($=S_1 + S_2$) must be numerically less than S_A ($=S_3 = 5/2$). The total cluster spin, $S_T = S_A + S_B = 1/2$, demands that S_B must be 2 or 3. The above condition that S_A is less than S_B dictates that the local spin for the Fe_1/Fe_2 pair must be $S_A = 2$. This conclusion is the same as that obtained from earlier EPR studies which revealed two similar couplings, J_{13} and J_{23} smaller than the third J_{12} (Kent et al., 1980). During the preparation of this manuscript, we became aware of a related

[4] E. T. Adman, private communication.

NMR study on oxidized *Dg* Fd which similarly shows that a single cysteine exhibits Curie-like and the other two cysteines exhibit anti-Curie like behavior.[5] A simulation of $\langle S_z \rangle$ based on a Heisenberg–Dirac–van Vleck spin coupling model, assuming $S_A = S_1 + S_2 = 2$ and $S_B = S_3 = 5/2$, showed[5] that the temperature behavior observed for the coordinated cysteines of oxidized *Dg* 3Fe Fd is reproduced with $J_{12} > J_{13} = J_{23}$. Modeling the magnitudes of the observed shifts in that study also permitted an estimate of the J values.

For the oxidized 3Fe center in the 7Fe Fd of *Peptococcus aerogenes* (*Pa*) and *Azotobacter vinelandii* (*Av*), earlier NMR studies showed that the sole pair of Curie-like low-field $C_\beta H$ signals arise from the same cysteine (Cheng et al., 1990). While the location of the signals of the remaining two cysteines of the 3Fe cluster remains controversial (Nagayama et al., 1980; Cheng et al., 1988), the absence of other Curie-like resolved signals indicates that our conclusions on the electronic/magnetic properties of the 3Fe cluster in hyperthermophilic Fd are also applicable to this protein. It is therefore apparent that the spin coupling hierarchy that has served so well as a basis for the interpretation of the magnetic/electronic properties of 4Fe clusters with valence-state differentiated iron pairs is also applicable to the states where the iron are valence-state equivalent. Since the local spin states in the $4Fe^{2.5+}$ systems are the same in oxidized HiPiP and reduced 4Fe Fd (Cammack et al., 1977), the coupling mechanism does not manifest itself strongly in the NMR properties, with the major influence being the anti-Curie behavior arising from the population of excited paramagnetic states (Bertini et al., 1990). The asymmetric coupling is clearly observed in the valence-state equivalent oxidized 3Fe Fd because the "local" or intermediate spin states are necessarily nonequivalent.

A question of significant interest that remains to be answered is whether the asymmetry (in terms of contributing cysteines) in the coupling of oxidized 3Fe clusters is the same as that in the reduced 3Fe cluster ($2Fe^{2.5+}$-$1Fe^{3.0+}$) (Papaefthymiou et al., 1987), or in the related reduced 4Fe cluster ($2Fe^{2.0+}$-$2Fe^{2.5+}$) (Park et al., 1991). The answer to this question can be addressed with current NMR methodology using *Pf* Fd and *Tl* Fd in their reduced 3Fe and 4Fe forms; such studies are in progress.

Sequence Control of the Magnetic Asymmetry. The available 2D COSY and NOESY maps of oxidized 3Fe Fd exhibit too many degeneracies to allow rapid sequence-specific assignments of the complete spectra. However, even in the absence of such assignments, the available data suggest that the cysteine exhibiting the Curie-like behavior (Cys C) does not have the same sequence origin (i.e., Cys I, III or IV in Figure 1C) in *Pf* Fd and *Tl* Fd. The strong structural homology for Fd of *Pf*, *Tl*, and *Dg* evidenced by the NOESY and 1D NOE contacts suggest very similar orientations of the individual Cys relative to the coordinated iron atoms. The pattern of the $C_\beta H$ contact shifts has been proposed (Poe et al., 1980) to reflect the orientation of a cysteine as defined by eq 1. However, the quantitative relationship depends on the nature of the unpaired spin delocalization mechanism, σ or π, that defines the angle ϕ in eq 1, but this spin mechanism is not known (Busse et al., 1991). A recent comparison of the sequence specifically assigned cysteine $C_\beta H$ contact shift pattern in oxidized HiPiP from *Chromatium vinosum* with the angles provided by the X-ray structure (Carter et al., 1974) showed that neither pure π nor σ accounts for the observed patterns (Nettesheim et al., 1992); both mechanisms may be operative. However, it is likely that the $C_\beta H$ contact shift patterns for two cysteine are the same only if their orientations are very similar. Conversely, significantly different $C_\beta H$ contact shift patterns must indicate different cysteine orientation.

Table I lists the contact shifts for the two $C_\beta Hs$ for each cysteine and the ratio for these contact shifts for the sequence specifically assigned Cys A (positions 17 in *Pf* Fd and 16 in *Tl* Fd). This ratio, which is defined as the shift for $C_\beta H$ divided by that for $C_\beta H'$, where $C_\beta H$, and $C_\beta' H$ are the protons further from and closer to the iron, is very similar (3.1 ± 0.4) for both proteins. For the other two cysteines, however, the ratio for either the labeled Cys B or Cys C differs substantially between the two proteins.[6] If the similarly labeled Cys residues (B or C) have the homologous sequence origins in the two proteins, the different ratios must reflect substantially different cluster geometries. However, the ratio of $C_\beta H$ contact shifts for Cys C in *Pf* and Cys B in *Tl* Fd (as well as for Cys B in *Pf* Fd and Cys C in *Tl* Fd) are quite similar (Table I). This similarity in shift ratio would argue that the Curie-like Cys C *does not originate in a structurally homologous Cys in the two proteins.* The different sequence origin for the unique Cys C in *Pf* Fd and *Tl* Fd is similarly supported by the relaxation properties of the $C_\beta H$ peaks. Thus, for two cysteines in each protein, the larger $C_\beta H$ contact shift is for the more weakly relaxed (further from the iron) protons i.e., Cys A and Cys B in *Pf* Fd and Cys A and Cys C in *Tl* Fd. For Cys C in *Pf* Fd and Cys B in *Tl* Fd, the larger contact shift arises from the $C_\beta H$ more strongly relaxed (closer to the iron) proton. The comparison of relaxation properties[6] of $C_\beta Hs$ therefore favor pairing Cys B in *Pf* Fd with Cys C in *Tl* Fd and Cys C in *Pf* Fd with Cys B in *Tl* Fd. These results suggest that the magnetic asymmetry may not be controlled by the sequence position of a cysteine but is instead modulated by tertiary interactions between the cluster and the protein matrix that reflect neighboring amino acid contacts. However, it is not clear that these magnetic asymmetries, which are based on small energy differnces, are functionally relevant.

The molecular heterogeneity detected in *Pf* Fd manifests itself most strongly for Cys C, less for Cys B, and insignificantly for Cys A and hence must reflect minor alternate conformations of the structure(s) including Cys I and IV (Figure 1). The failure to detect such low-temperature broadening or splitting of the Cys C and Cys B peaks in *Tl* Fd could arise from either the absence of this heterogeneity or simply a faster interconversion rate. It should be noted that whatever the molecular heterogeneity in the oxidized 3Fe form of *Pf* Fd, it exerts only minimal influence on the cysteinyl $C_\beta H$ contact shift patterns for the alternate forms. While this heterogeneity complicates the sequence-specific assignment of *Pf* Fd, such assignments, when complete, should not only provide the identity of the Curie-like Cys C in the sequence but also elucidate the nature of the alternative conformations of the structure(s) involving Cys I and IV.

ACKNOWLEDGMENT

We are indebted to J. J. G. Moura for providing a copy of their manuscript prior to publication and to E. T. Adman for providing the refined crystal coordinates of *D. gigas* ferredoxin.

[5] A. L. Maceda, I. Moura, J. LeGall, J. J. G. Moura, and B. H. Huynh, submitted for publication.

[6] The conclusion that the shift ratios of Cys B of *Pf* Fd and Cys C of *Tl* Fd (or Cys C of *Pf* Fd and Cys B of *Tl* Fd) are more similar than either the Cys B or Cys C in both proteins is valid even if the inverse of the shift ratio in Table I are used. Hence, the shift ratios and relaxation properties do not provide independent information on the similarities of cysteine environments in the two proteins.

SUPPLEMENTARY MATERIAL AVAILABLE

Three figures showing the DQF-COSY/NOESY split diagonal spectrum for the diamagnetic region of *Tl* Fd and 1D NOE difference traces for hyperfine shifted cysteine $C_\beta H$ resonances for *Pf* Fd and *Tl* Fd (3 pages). Ordering information is given on any current masthead page.

REFERENCES

Adams, M. W. W. (1992) *Adv. Inorg. Chem. 38*, 341–396.

Aono, S.; Bryant, F. O., & Adams, M. W. W. (1989) *J. Bacteriol. 171*, 3433–3439.

Banci, L., Bertini, I., & Luchinat, C. (1990) *Struct. Bonding 72*, 113–135.

Banci, L., Bertini, I., Briganti, F., Luchinat, C., & Scozzafava, A. (1991a) *Inorg. Chem. 30*, 4517–4524.

Banci, L., Bertini, I., Briganti, F., Scozzafava, A., Vicens Oliver, M., & Luchinat, C. (1991b) *Inorg. Chem. Acta 180*, 171–175.

Bax, A. (1982) *Two-dimensional NMR in Liquids*, Reidel Publishing Co., Dordrecht, The Netherlands.

Beinert, H. (1990) *FASEB J. 4*, 2483–2491.

Bertini, I., Briganti, F., Luchinat, C. & Scozzafava, A. (1990) *Inorg. Chem. 29*, 1874–1880.

Bertini, I., Briganti, F., Luchinat, C., Scozzafava, A., & Sola, M. (1991) *J. Am. Chem. Soc. 113*, 1237–1245.

Bertini, I., Briganti, F., Luchinat, C., Messori, L., Mannanni, R., Scozzafava, A., & Vallini, G. (1992a) *Eur. J. Biochem. 204*, 831–835.

Bertini, I., Capozzi, F., Ciurli, S., Luchinat, C., Messori, L., & Piccioli, M. (1992b) *J. Am. Chem. Soc. 114*, 3332–3340.

Bryant, F. O., & Adams, M. W. W. (1989) *J. Biol. Chem. 264*, 5070–5079.

Busse, S. C., La Mar, G. N., & Howard, J. B. (1991) *J. Biol. Chem. 266*, 23714–23723.

Cammack, R., Dickson, D. P. E., & Johnson, C. E. (1977) in *Iron Sulfur Proteins* (Lovenberg, W., Ed.) Vol. III, pp 283–330, Academic Press, New York.

Carter, C. W., Kraut, J., Freer, S. T., Xuong, N. H., Alden, R. A., & Bartsch, R. G. (1974) *J. Biol. Chem. 249*, 4212–4225.

Cheng, H., Grohmann, K., & Sweeney, W. V. (1990) *J. Biol. Chem. 265*, 12388–12392.

Conover, R. C., Kowal, A. T., Fu, W., Park, J.-B., Aono, S., Adams, M. W. W., & Johnson, M. K. (1990a) *J. Biol. Chem. 265*, 8533–8541.

Conover, R. C., Park, J.-B., Adams, M. W. W., & Johnson, M. K. (1990b) *J. Am. Chem. Soc. 112*, 4562–4564.

Conover, R. C., Park, J.-B., Adams, M. W. W., & Johnson, M. K. (1991) *J. Am. Chem. Soc. 113*, 2799–2800.

Cowan, M., & Sola, M. (1990) *Biochemistry 29*, 5633–5637.

Day, E. P., Peterson, J., Bonovoisin, J. J., Moura, I., & Moura, J. J. G. (1988) *J. Biol. Chem. 263*, 3684–3689.

Dickson, D. P. E., Johnson, C. E., Commack, R., Evans, M. C. J., Hall, D. O., & Rao, K. K. (1974) *Biochem. J. 139*, 105–108.

Dugad, L. B., La Mar, G. N., Banci, L., & Bertini, I. (1990) *Biochemistry 29*, 2263–2271.

Dunham, W. R., Palmer, G., Sands, R. H., & Bearden, R. J. (1971) *Biochim. Biophys. Acta 253*, 373–384.

Emptage, M. H., Kent, T. A., Huynh, B. H., Rawlings, J., Orme-Johnson, W. H., & Münck, E. (1980) *J. Biol. Chem. 255*, 1793–1796.

Fiala, G., & Stetter, K. O. (1986) *Arch. Microbiol. 145*, 56–61.

Gibson, J. F., Hall, D. O., Thornley, J. H. M., & Wheatley, F. R. (1966) *Proc. Natl. Acad. Sci. U.S.A. 56*, 987–992.

Howard, J. B., & Rees, D. C. (1991) *Adv. Protein Chem. 42*, 99199–99208.

Huynh, B. H., Moura, J. J. G., Moura, I., Kent, T. A., Le Gall, J., Xavier, A. V., & Münck, E. (1980) *J. Biol. Chem. 255*, 3242–3244.

Inubushi, T., & Becker, G. D. (1983) *J. Magn. Reson. 51*, 128–133.

Johnson, C. E. (1986) *J. Inorg. Biochem. 28*, 207–215.

Kent, T. A., Huynh, B. H., & Münck, E. (1980) *Proc. Natl. Acad. Sci. U.S.A. 77*, 6574–6576.

Kissinger, C. R., Adman, E. T., Sieker, L. C. & Jensen, L. H. (1988) *J. Am. Chem. Soc. 110*, 8721–8723.

Kissinger, C. R., Adman, E. T., Sieker, L. C., Jensen, L. H., & Le Gall, J. (1989) *FEBS Lett. 244*, 447–450.

La Mar, G. N., & de Ropp, J. S. (1993) in *Biological Magnetic Resonance* (Berlinger, L. J., & Reuben, J., Eds.), Vol. 12, Plenum Press, New York (in press).

Lovenberg, W., Ed. (1973) *Iron Sulfur Proteins*, Vol. III, Academic Press, New York.

Marion, D., & Wüthrich, K. (1983) *Biochem. Biophys. Res. Commun. 113*, 967–974.

Middleton, P., Dickson, D. P. E., Johnson, C. E., & Rush, J. D. (1978) *Eur. J. Biochem. 88*, 135–141.

Middleton, P., Dickson, D. P. E., Johnson, C. E., & Rush, J. D. (1980) *Eur. J. Biochem. 104*, 289–296.

Moss, T. H., Bearden, A. J., Bartsch, R. G., Cusanovich, M. A. & San Pietro, A. (1968) *Biochemistry 7*, 1591–1596.

Moura, J. J. G., Xavier, A. V., Bruschi, M., & Le Gall, J. (1977) *Biochem. Biophys. Acta 459*, 278–289.

Moura, J. J. G., Moura, I., Kent, T. A., Lipscomb, J. D., Huynh, B. H., Le Gall, J., Xavier, A. V., & Münck, E. (1982) *J. Biol. Chem. 257*, 6259–6267.

Münck, E., Papaefthymiou, V., Sererus, K. K., & Girerd, J.-J. (1988) in *Metal Clusters in Proteins*, (Que, L., Ed.) ACS Symposium Series pp 302–325, American Chemical Society, Washington, DC.

Nagayama, K., Ohmori, D., Imai, T., & Oshima, T. (1986) in *Iron Sulfur Protein Research* (Matsubara, H., Kasube, Y., & Wada, K., Eds.) pp 125–138, Japan Science Society Press, Tokyo.

Nettesheim, D. G., Harder, S. R., Feinberg, B. A., & Otvos, J. D. (1992) *Biochemistry 31*, 1234–1244.

Neuhaus, D., & Williamson, M. (1989) *The Nuclear Overhauser Effect*, VCH Publishers, New York.

Neuner, A., Jannasch, H. W., Belkin, S., & Stetter, K. O. (1990) *Arch. Microbiol. 153*, 205–207.

Noodleman, L. (1988) *Inorg. Chem. 27*, 3677–3679.

Noodleman, L. (1991) *Inorg. Chem. 30*, 246–264.

Papaefthymiou, V., Girerd, J. J., Moura, I., Moura, J. J. G., & Münck, E. (1987) *J. Am. Chem. Soc. 109*, 4703–4710.

Park, J.-B., Fan, C., Hoffman, B. M., & Adams, M. W. W. (1991) *J. Biol. Chem. 266*, 19351–19356.

Poe, M., Phillips, W. D., McDonald, C. C., & Lovenberg, W. (1970) *Proc. Natl. Acad. Sci. U.S.A. 65*, 797–804.

Sandström, J. (1982) *Dynamic NMR Spectroscopy*, Academic Press, New York.

Skjeldal, L., Westler, W. M., Oh, B.-H., Krezel, A. M., Holden, H. M., Jacobsen, B. L., Rayment, I., & Markley, J. L. (1991) *Biochemistry 30*, 7363–7368.

Spiro, T. G., Ed. (1982) *Iron Sulfur Proteins*, Vol. IV, John Wiley, New York.

Thompson, A. J. (1985) in *Metalloproteins* (Hanson, P., ed.) Part I, pp 79–120, Verlag Chemie, Weinheim.

Thompson, A. J., Robinson, A. E., Johnson, M. K., Moura, J. J. G., Moura, I., Xavier, A. V., & LeGall, J. (1981) *Biochim. Biophys. Acta 670*, 93–100.